Journal of Power Sources 195 (2010) 2918–2923

Contents lists available at ScienceDirect

Journal of Power Sources

journal homepage: www.elsevier.com/locate/jpowsour

Short communication

Structure, morphology, and cathode performance of $Li_{1-x}[Ni_{0.5}Mn_{1.5}]O_4$ prepared by coprecipitation with oxalic acid

Dongqiang Liu, Jiantao Han, John B. Goodenough*

Texas Materials Institute, ETC 9.184, University of Texas at Austin, 1 University Station, C2200, Austin, TX 78712, United States

ARTICLE INFO

Article history:
Received 20 October 2009
Received in revised form 3 November 2009
Accepted 4 November 2009
Available online 13 November 2009

Keywords:
Cathode
$Li_{1-x}Ni_{0.5}Mn_{1.5}O_4$
Coprecipitate method
Octahedral shape

ABSTRACT

The cathode materials $Li_{1-x}[Ni_{0.5}Mn_{1.5}]O_4$ prepared by coprecipitation from acetate solution by oxalic acid and annealing at 900 °C in air had the preferred disordered Ni and Mn on the 16d octahedral sites of a spinel $Fd\bar{3}m$ structure. The coprecipitation method provides better crystallinity than the $Fd\bar{3}m$ phase previously obtained by quenching from the melt. Polycrystalline octahedral-shaped particles with smooth surfaces contained trace amounts of a $Li_yNi_{1-y}O$ impurity that introduced some Mn(III) into the spinel phase. Half-cells cycled at 0.2 C rate between 3.5 and 4.8 V versus Li exhibited a flat voltage $V \approx 4.7$ V with a small step at $x \approx 0.5$ and a capacity at room temperature of 130 mAh g^{-1} that showed no fade after 50 cycles. A small capacity fade was initiated with a cut-off voltage $\geq$4.9 V; a significant capacity loss between 2 and 5 C cycling rates was reversible to 134 mAh g^{-1} on returning to 0.1 C after 50 cycles at 10 C between 3.5 and 5.0 V.

Published by Elsevier B.V.

1. Introduction

The growing interest in Li^+-ion high-power batteries has stimulated a world-wide search for a high-capacity cathode material capable of fast discharge rates over many charge/discharge cycles and having the energy of its active redox couple well-matched to the highest occupied molecular orbital (HOMO) of a liquid carbonate electrolyte; this HOMO is about 4.3 eV below the Fermi energy of a lithium anode, and the electrolyte decomposes above 4.9 V verses lithium. Much attention has been given to the spinel $Li_{1-x}[Ni_{0.5}Mn_{1.5}]O_4$ because it provides access to the Ni(IV)/Ni(III) couple below 4.8 V versus lithium [1,2]. The access to two redox couples of Ni without a significant step between them is possible because these couples are both pinned at the top of the O-2p bands [3]. A small step between the redox couples is due to the appearance of a $Li_{0.5}[Ni_{0.5}Mn_{1.5}]O_4$ phase containing ordered Li^+ ions; this ordered Li^+-ion phase creates a two-phase region between it and $Li[Ni_{0.5}Mn_{1.5}]O_4$ on one side and between it and $[Ni_{0.5}Mn_{1.5}]O_4$ on the other side [4–6]. These three cubic phases have distinguishable lattice parameters, and the two-phase regions give flat *V(x)* profiles with a reversible Li extraction/insertion reaction. Moreover, annealing at 700 °C was found to order the Ni(II) and Mn(IV) ions on the octahedral sites, changing the structure from face-centered-cubic spinel ($Fd\bar{3}m$) to primitive simple cubic ($P4_332$) [6]. Ordering of the Ni(II) and Mn(IV) raises by 0.02 eV the *V(x)* profiles of $Li_{1-x}[Ni_{0.5}Mn_{1.5}]O4$; also lowers the rate capability.

In the layered $Li_{1-x}Co_{0.15}Ni_{0.85}O_2$, the *intrinsic* [7] voltage limit is 3.8 V versus Li; for $x > 0.8$, the holes in the Ni(IV)/Ni(III) couple become trapped in surface peroxide ions with subsequent loss of O_2. However, in the spinel system $Li_{1-x}[Ni_{0.5}Mn_{1.5}]O_4$, the Li^+ ions occupy tetrahedral sites rather than octahedral sites, which lowers the energy of all occupied electronic states by 1 eV. This shift has been demonstrated [8] by a shift in the Mn(IV)/Mn(III) couple from 3.0 V versus lithium in $Li_{1+x}[Mn_2]O_4$ to 4.0 V in $Li_{1-x}[Mn_2]O_4$. Moreover, the interaction between the Mn(IV) and Ni(IV) redox couples in $[Ni_{0.5}Mn_{1.5}]O_4$ raises the Ni(IV)/Ni(III) couple just enough to allow complete access to the Ni(IV)/Ni(III) couple in the spinel framework. On the other hand, at 4.9 V versus lithium, the Ni(IV)/Ni(III) couple is at the energy of the degradation of the electrolyte $LiPF_6$ in ethylene carbonate/diethyl carbonate (EC/DEC); decomposition of the electrolyte occurs at a $V \geq 4.9$ V versus Li at room temperature; at higher temperatures, oxidation of the electrolyte at $V \approx 4.8$ V may be a problem. Cation substitutions that might raise the Ni (IV)/Ni (III) redox energy [9,10] and passivating coatings [11] continue to be investigated.

Another problem has been a difficulty to prepare a pure, stoichiometric $Li_{1-x}[Ni_{0.5}Mn_{1.5}]O_4$ spinel; formation of $Li_yNi_{1-y}O$ appears as a second phase, which deteriorates the electrochemical behavior [12–15]. Loss of nickel from the spinel phase introduces Mn(III) ions; these ions introduce a step in the *V(x)* profile at 4.0 V versus Li. The presence of the impurity phase reduces the capacity of the plateaus at ca. 4.7 V and may impede the motion of any inter-

* Corresponding author. Tel.: +1 512 471 1646; fax: +1 512 471 7681.
E-mail address: jgoodenough@mail.utexas.edu (J.B. Goodenough).

0378-7753/$ – see front matter. Published by Elsevier B.V.
doi:10.1016/j.jpowsour.2009.11.024

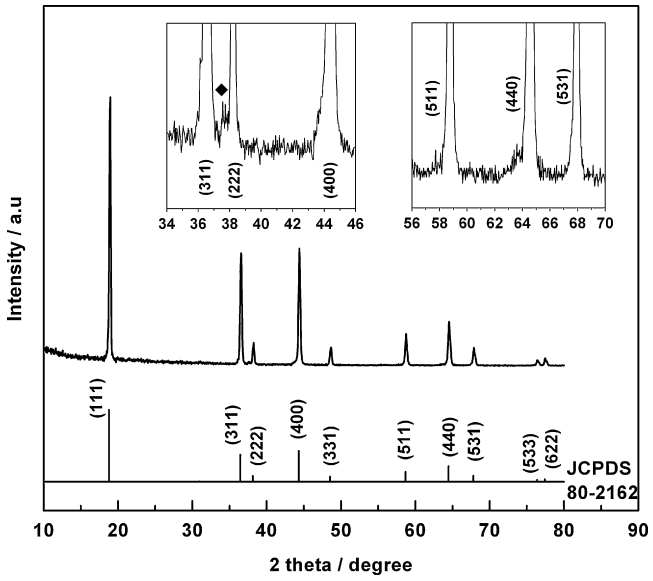

Fig. 1. XRD pattern of the final $LiNi_{0.5}Mn_{1.5}O_4$ sample.

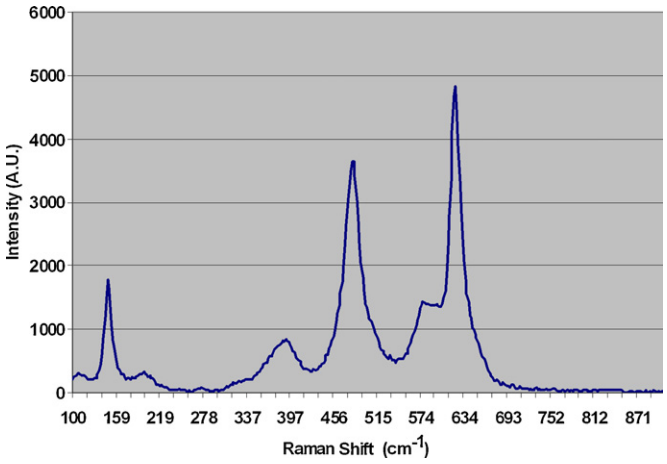

Fig. 2. Raman spectra of the $LiNi_{0.5}Mn_{1.5}O_4$ powders.

face between two coexisting spinel phases. In addition, we note that in the spinel system $Li_{1-x}[Mn_2]O_4$, a surface disproportionation reaction 2Mn(III) = Mn(II) + Mn(IV) appears to be associated with an ordered $Li_{0.5}[Mn_2]O_4$ phase [16] and dissolution of Mn(II) ions into the electrolyte creates an *irreversible* capacity loss on repeated cycling.

Previous synthesis routes have included molten-salt reaction, reaction via a sol–gel, and reaction after coprecipitation [12–14]. In the present work, well-crystallized, octahedral-shaped nominal $Li[Ni_{0.5}Mn_{1.5}]O_4$ particles with $Fd\bar{3}m$ space group were obtained after coprecipitation from a metal-acetate solution by adding oxalic acid. The particles were characterized by X-ray diffraction

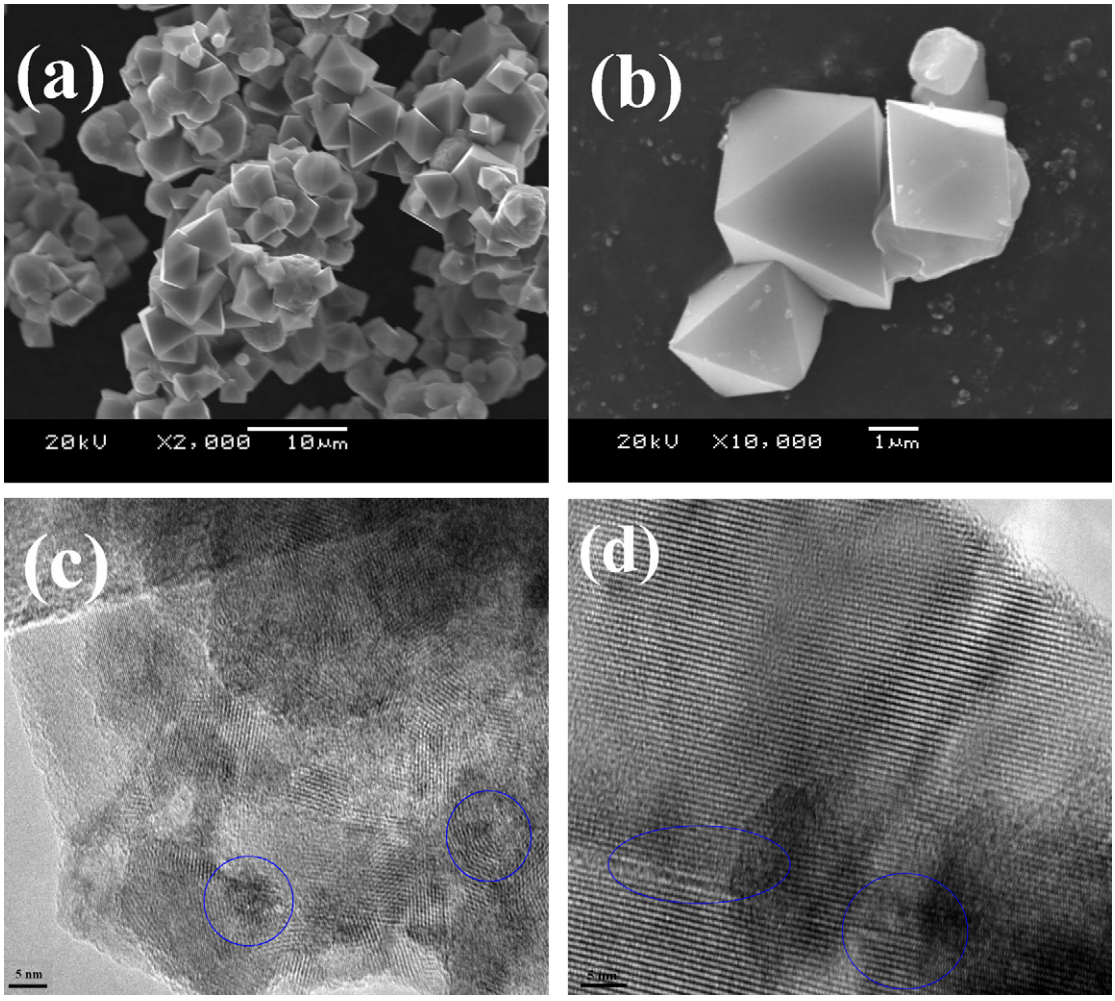

Fig. 3. SEM and TEM images of the octahedral-shape $LiNi_{0.5}Mn_{1.5}O_4$ particles.

(XRD), Raman spectroscopy, transmission and scanning electron microscopy (TEM and SEM). The electrochemical properties of the octahedral-shaped particles were obtained by galvanostatic charge/discharge cycles at different cut-off voltages and discharge currents. At room temperature, capacity loss on cycling only commenced for cut-off voltages greater than 4.8 V versus lithium; a capacity of about 138 mAh g^{-1} was obtained in the range 3.5–4.9 V.

2. Experimental

2.1. Synthesis

Stoichiometric amounts of manganese, lithium, and nickel acetates (99% Aldrich) were first dissolved in distilled water and stirred for 1 h. Oxalic-acid solution was then added dropwise under stirring to obtain a green precipitate. The molar ratio of oxalic acid to metal ions was controlled to be 1:1. The precipitate solution was continually stirred for 1 h before being dried at 50 °C overnight with constant stirring. The dried precipitate was preheated at 500 °C for 6 h and then ground for 30 min. The preheated powder was pressed into pellets (20 mm dia. and *ca.* 5 mm thick) and annealed at 900 °C for 24 h in air for better crystal growth. This synthetic route provides good crystallization of the $Fd\bar{3}m$ phase with disordered Ni and Mn.

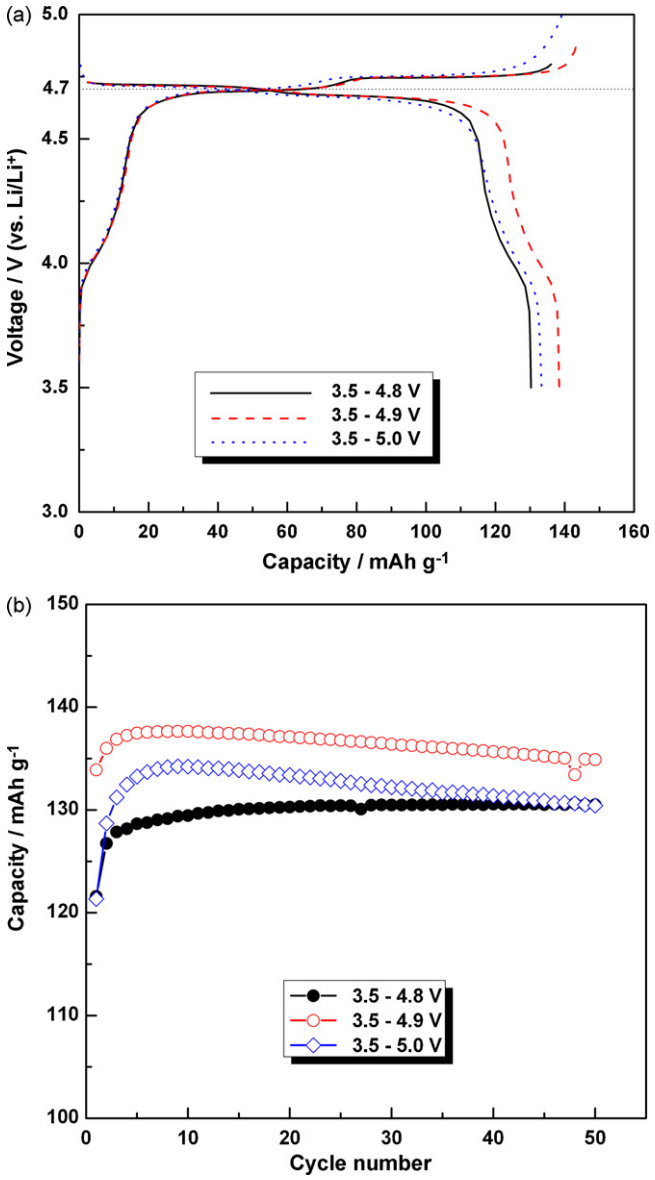

Fig. 4. Voltage profiles (a) and cycling performance (b) of the $Li/LiNi_{0.5}Mn_{1.5}O_4$ cells between different cut-off potentials. The cells were cycled at the current rate of ~0.2 C; the cathode was about 0.05 mm thick.

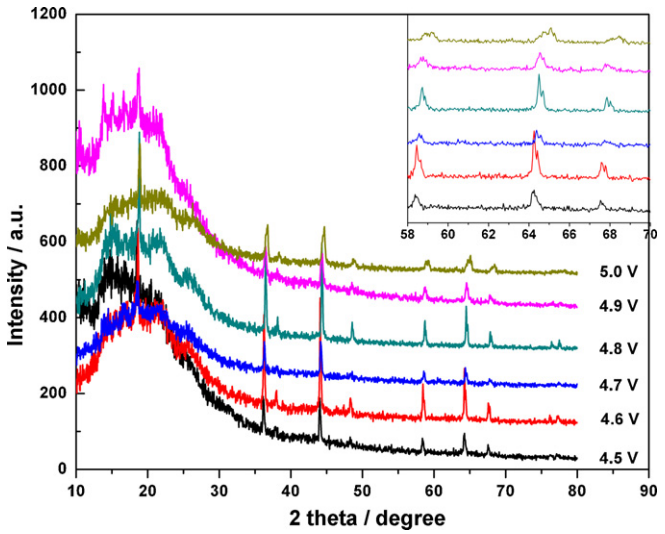

Fig. 5. XRD patterns of the electrodes at various depths of charge. Inset shows the magnified peaks between $2\theta = 58–70°$.

2.2. Characterization

Powder XRD data were collected with a Philips X-ray diffractometer equipped with Cu Kα radiation in steps of 0.04° with a step time of 2 s over the range $10° < 2\theta < 80°$. The *ex situ* XRD of electrodes were obtained from samples prepared inside a glove box by carefully opening a cell and placing the electrode material on a glass sample holder before covering the sample with an amorphous plastic tape to avoid exposure to air. TEM images were obtained with an electron microscope (Hitachi model H-9000, 300 kV). The TEM samples were treated ultrasonically in a solution of isopropyl alcohol and then deposited on a silica substrate. The particle morphologies before and after charge/discharge were characterized by SEM (JEOL JSM-5610). Raman spectra were obtained with a Jobin-Yuon U1000 double-pass spectrometer equipped with a cooled, low-noise photomultiplier tube (ITT FW130).

2.3. Performance

Electrochemical performances of half-cells were evaluated with a standard CR2032 coin cell composed of a spinel cathode, lithium anode, a Celgrade polypropylene separator, and $LiPF_6$ in 1:1 EC/DEC as electrolyte. The cathode was prepared by mixing 75 wt.% spinel oxide with 20 wt.% acetylene black and 5 wt.% polytetrafluoroethylene (PTFE) binder; the mixture was rolled into thin sheets that were punched into 1-cm-diameter circular discs. A typical electrode mass and thickness were 4–8 mg and 0.02–0.06 mm. All cells were fabricated in an argon-filled glove box. The cells were aged for 12 h before charge/discharge to ensure full absorption of the electrolyte into the electrode. Cells were galvanstatically cycled under different conditions in an Arbin Instruments (Arbin BT-200) tester.

3. Results

The XRD pattern of the final sample, Fig. 1, corresponds to that of a high-purity spinel with only a trace of the $Li_yNi_{1-y}O$ rock-salt impurity giving a weak-intensity reflection at *ca.* $2\theta = 37.5°$,

Fig. 1 inset; no other reflections of this impurity were detected at *ca.* $2\theta = 43.5^\circ$, 63.5°, or 68.2°. Moreover, no superstructure peaks were detected at $2\theta = 15.3^\circ$, 39.7°, 45.7°, 57.5°, or 65.6°, the positions considered to represent an ordering of the Ni(II) and Mn(IV) ions in the $P4_332$ structure [17]. All the diffraction peaks can be indexed in the space group $Fd\bar{3}m$ (JCPDS No. 80-2162) of a cubic spinel. The negligible intensity of the diffraction peak (220) at $2\theta = 26^\circ$ can be attributed to the absence of transition-metal ions in the *8a* tetrahedral sites [17].

Fig. 2 shows a typical Raman spectrum of our $Li[Ni_{0.5}Mn_{1.5}]O_4$ powder. The 625 cm^{-1} peak assigned to the symmetric Mn–O stretching vibration of the MnO_6 octahedra in $Li[Mn_2]O_4$ is shifted to 635 cm^{-1}. The new features at 397 and 496 cm^{-1} are strong and can therefore be assigned unequivocally to the Ni–O stretching mode. The frequency shift of the Mn–O stretching mode is attributed to (1) the increased mean valence state of the Mn ions and (2) a smaller unit-cell volume. None of the peaks characteristic [18] of ordering of the Ni(II) and Mn(IV) in space group $P4_332$ (or $P4_132$), *viz.* at 202, 240, 599, and 611 cm^{-1}, were detected, which is a further indication that the Ni(II) and Mn(IV) of our samples were disordered over the 16d sites of the $Fd\bar{3}m$ spinel.

Not only the crystal structure, but also the crystallite size and morphology are important for the electrochemical performance of a cathode material in a Li^+-ion secondary battery [19]. Fig. 3 shows typical SEM and TEM images used to characterize the crystallite size and surface morphology of our $Li[Ni_{0.5}Mn_{1.5}]O_4$ spinel particles. Fig. 3a shows that the samples are not only well crystallized, but also are without serious agglomeration after annealing at 900 °C for 24 h in air. Most of the particles were <5 μm in diameter with a perfect octahedral shape showing smooth surfaces, Fig. 3b. However, the TEM images of Fig. 3c and d indicate a polycrystalline microstructure within the particles with nano-size domains (5–15 nm) of different orientations, some disordered areas, and bent lattice fringes.

Fig. 4 shows voltage profiles and cycling performance of $Li/Li[Ni_{0.5}Mn_{1.5}]O_4$ half-cells cycled, respectively, between 3.5 and 4.8, 3.5 and 4.9, 3.5 and 5.0 V at a 0.2 C rate. The voltage profiles of Fig. 4a show a small step at 4.1 V characteristic of the Mn(IV)/Mn(III) redox couple, indicating the presence of some Mn(III) in the spinel as a result of loss of Ni to the $Li_yNi_{1-y}O$ rock-salt phase. The flat portion of the profile just below 4.7 V corresponds to the Ni(III)/Ni(II) redox reaction for disordered $Fd\bar{3}m$; it compares with ~4.72 V for the ordered $P4_332$ spinels [20]. The other plateau at ~4.71 V reflects the Ni(IV)/Ni(III) couple in the two-phase region containing $Li_{0.5}[Ni_{0.5}Mn_{1.5}]O_4$ and $[Ni_{0.5}Mn_{1.5}]O_4$. Between 3.5 and 4.8 V, the cell delivered a discharge capacity of about 130 mAh g^{-1} with a remarkable capacity retention of 100% over 50 cycles. Between 3.5 and 4.9 V, the cell capacity was 138 mAh g^{-1}, but a 1.44% loss was observed after 50 cycles. With a cut-off voltage of 5.0 V, the cell showed a capacity of 134 mAh g^{-1} with a capacity rentention of 96.3% after 50 cycles.

Fig. 5 presents selected XRD patterns of the $Li_{1-x}[Ni_{0.5}Mn_{1.5}]O_4$ electrodes at different depths of charge. The diffraction peaks clearly shift to higher angles as Li is removed with a splitting of the lines showing the coexistence of two cubic phases as has previously been reported [21]. However, in Fig. 5 all the peaks can be indexed in space group $Fd\bar{3}m$; no superstructure peaks emerge on passing from one cubic phase to the next at room temperature.

Fig. 6 compares the structures and morphologies of the electrode particles after 50 cycles at different cut-off voltages. Before cycling, the typical particle morphology was octahedral with smooth surfaces, Fig. 6a. After 50 cycles between 3.5 and 4.8 V, Fig. 6b, the particle surfaces were still smooth despite some small changes of particle size and morphology. In contrast to Fig. 6a and b, the images of Fig. 6c and d, corresponding to cut-off voltages of 4.9 and 5.0 V,

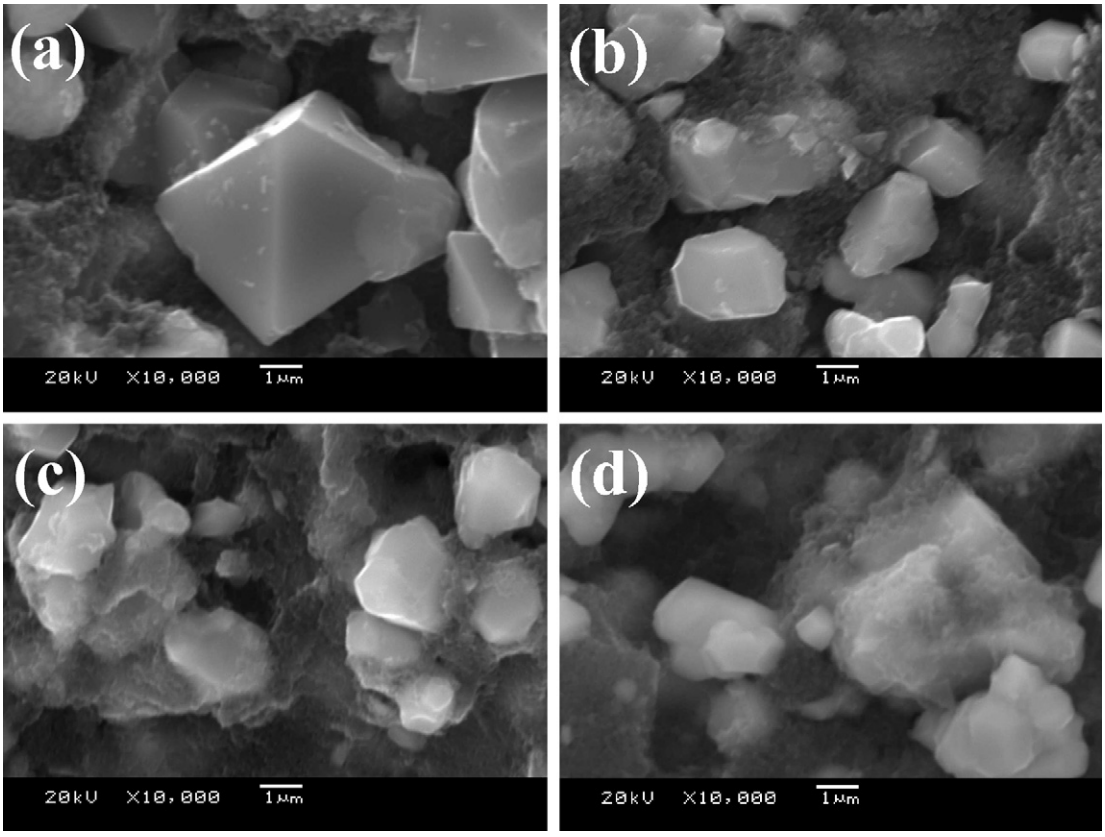

Fig. 6. SEM images of electrodes before and after cycling at different cut-off voltages.

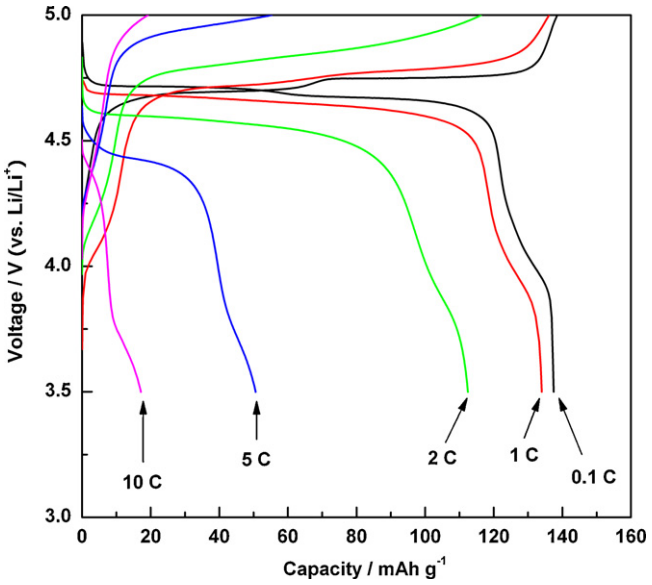

Fig. 7. Voltage curves of the octahedral-shape $LiNi_{0.5}Mn_{1.5}O_4$ samples at various C rates. The cells were cycled between 3.5 and 5 V.

show particles of irregular shape with a roughness that increases with the cut-off voltage.

The octahedral-shaped $Li[Ni_{0.5}Mn_{1.5}]O_4$ spinels were also cycled at different rates from 0.1 to 10 C and then back to 0.1 C with a cut-off voltage of 5.0 V. The several voltage profiles are shown in Fig. 7, the capacity retention in Fig. 8. A reversible capacity loss from 138 mAh g^{-1} at 0.1 C increases dramatically from the 2 C to the 5 C rate, but capacity retention remained even at the 10 C rate and capacity was recovered on returning to the 0.1 C rate. The reversibility of the capacity shows that the degradation was not due to an irreversible structural change, but to a diffusion-limited end-of-life polarization resulting from a slow Li^+-ion diffusion either across the electrolyte/electrode interface or within the bulk of the particles. Fig. 9 compares the dQ/dV versus V data at various rates, where $Q = \int I dt$ from $t = 0$ at 3.5 V to t at (V–3.5) V. The difference between the anodic and cathodic peaks increases with the rate of charge/discharge, which indicates an increase in the ohmic polarization loss due to Li^+-ion diffusion within the cell.

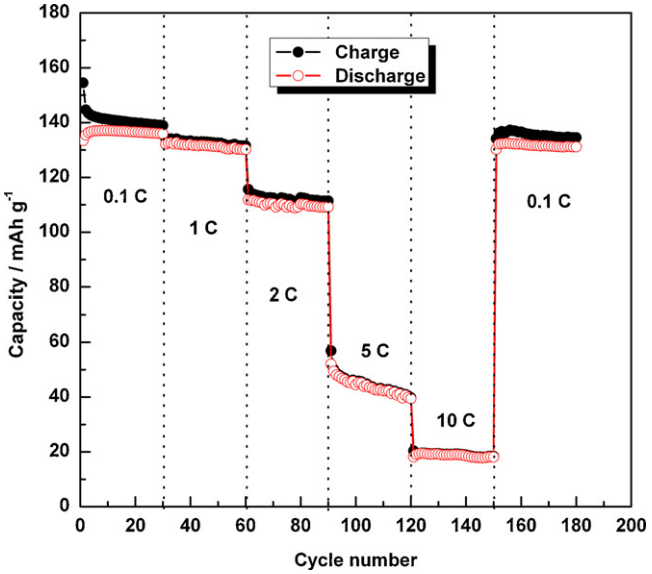

Fig. 8. Cyclabilities of the octahedral-shape $LiNi_{0.5}Mn_{1.5}O_4$ at various C rates.

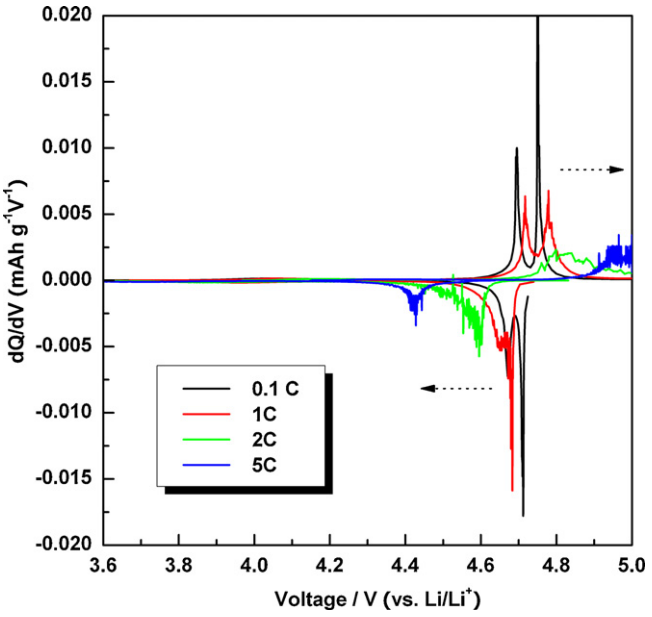

Fig. 9. dQ/dV versus voltage of the octahedral-shape $LiNi_{0.5}Mn_{1.5}O_4$ at various C rates.

4. Conclusions

Synthesis of nominal $Li[Ni_{0.5}Mn_{1.5}]O_4$ by a coprecipitation that is assisted by oxalic acid results in fine powders of octahedral shape after an anneal in air at 900 °C for 24 h. The resulting spinel structure shows that the Ni(II) and Mn(IV) ions are disordered over the 16d octahedral sites of the $Fd\bar{3}m$ spinel structure. This disorder persists on cycling at room temperature between $Li[Ni_{0.5}Mn_{1.5}]O_4$ and $[Ni_{0.5}Mn_{1.5}]O_4$, but a small step in the flat voltage profile at *ca.* 4.7 V versus Li signals stabilization of $Li_{0.5}[Ni_{0.5}Mn_{1.5}]O_4$ as an intermediate cubic phase distinguishable from the two end-member cubic phases. A small step at 4.1 V versus Li as well as XRD evidence of some $Li_yNi_{1-y}O$ shows the presence of some Mn(III) in the spinel phase as a result of Ni loss. At a cut-off voltage of 4.8 V, excellent reversibility of a 130 mAh g^{-1} capacity is to be compared with a theoretical 147 mAh g^{-1} for a spinel containing $Ni_{0.5}Mn_{1.5}$. We therefore conclude that the Ni(IV)/Ni(III) redox couple is fully accessed before the *intrinsic* capacity limit of the spinel is reached. This result was obtained without any cation substitution or surface coating of the particles. The initiation of an irreversible capacity loss at a cut-off voltage of 4.9 V therefore implies that degradation of the electrolyte begins at room temperature at a $V \geq 4.9$ V versus Li, consistent with polymerization or decomposition of organic electrolytes for voltages $\leq$5.0 V versus Li [22].

From a comparison of these data with those for the layered $Li_{1-x}NiO_2$ system, we further conclude that an interaction between the Mn(IV) and Ni(IV) ions raises the energy of the Ni(IV)/Ni(III) couple sufficiently to allow complete access to the couple before the intrinsic oxidation limit of the oxide is reached. Moreover, the data also demonstrate that shifting the Li^+ ions from octahedral to tetrahedral sites stabilizes by 1 eV not only the Ni(III)/Ni(II) and Ni(IV)/Ni(III) couples, but also the top of the O-2p bands at which these couples are pinned. This 1 eV shift is similar to the shift of the Mn(IV)/Mn(III) couple between the $Li_{1-x}[Mn_2]O_4$ and the $Li_{1+x}[Mn_2]O_4$ spinel frameworks.

The disappointing rate capability for insertion of Li into $[Ni_{0.5}Mn_{1.5}]O_4$ may reflect a slow bulk diffusion of the boundary between two cubic phases impeded by grain boundaries, disordered regions, the impurity phase, and/or slow diffusion across an SEI layer. Whether the rate capability can be improved by the syn-

thesis of smaller single-domain particles free of impurities remains to be investigated as, also, does the performance at different temperatures.

Acknowledgements

Financial support from Hydro-Québec as well as from the Robert A. Welch Foundation, Grant #F-1066, is gratefully acknowledged.

References

[1] T. Ohzuku, S. Takeda, M. Iwanaga, J. Power Sources 81–82 (1999) 90.
[2] K. Amine, H. Tukamoto, H. Yasuda, Y. Fujita, J. Power Sources 68 (1997) 604.
[3] J.B. Goodenough, in: W. Van Schalkwijk, B. Scrosati (Eds.), Advances in Lithium-Ion Batteries, Kluwer Adademic/Plenum Publishers, 2002, p. 147.
[4] J.-H. Kim, S.-T. Myung, C.S. Yoon, S.G. Kang, Y.-K. Sun, Chem. Mater. 16 (2004) 906.
[5] K. Ariyoshi, Y. Iwakoshi, N. Nakayama, T. Ohzuku, J. Electrochem. Soc. 151 (2004) A296.
[6] J.-H. Kim, C.S. Yoon, S.-T. Myung, J. Prakash, Y.-K. Sun, Electrochem. Solid-State Lett. 7 (2004) A216.
[7] S. Venkatramen, Y. Shin, A. Manthiram, Electrochem. Solid-State Lett. 6 (2003) A9.
[8] M.M. Thackeray, P.J. Johnson, L.A. DePicciotto, P.G. Bruce, J.B. Goodenough, Mater. Res. Bull. 19 (1984) 179.
[9] S. Rajakumar, R. Thirunakaran, A. Sivashanmugam, Y. Jun-ichi, S. Gopukumara, J. Electrochem. Soc. 156 (2009) A246.
[10] K. Hong, Y. Sun, J. Power Sources 109 (2002) 427.
[11] J. Liu, A. Manthiram, J. Electrochem. Soc. 156 (2009) A66.
[12] J.-H. Kim, S.-T. Myung, Y.-K. Sun, Electrochim. Acta 49 (2004) 219.
[13] Q. Zhong, A. Bonakdarpour, M. Zhang, Y. Gao, J.R. Dahn, J. Electrochem. Soc. 144 (1997) 205.
[14] R. Alcantara, M. Jaraba, P. Lavela, J.L. Tirado, Electrochim. Acta 47 (2002) 1829.
[15] K. Amine, H. Tukamoto, H. Yasuda, Y. Fujita, J. Electrochem. Soc. 143 (1996) 1607.
[16] W. Choi, A. Manthiram, Electrochem. Solid-State Lett. 9 (2006) A245.
[17] R. Alcantara, M. Jaraba, P. Lavela, J.L. Tirado, Chem. Mater. 15 (2003) 2376.
[18] N. Amdouni, K. Zaghib, F. Gendron, A. Mauger, C.M. Julien, Ionics 12 (2006) 117.
[19] Y. Shin, A. Manthiram, Electrochim. Acta 48 (2003) 3583.
[20] M. Kunduraci, G.G. Amatucci, J. Power Sources 165 (2007) 359.
[21] S.-T. Myung, S. Komaba, N. Kumagai, H. Yashiro, H.-T. Chung, T.-H. Cho, Electrochim. Acta 47 (2002) 2543.
[22] M. Winter, R.J. Brodd, Chem. Rev. 104 (2004) 4245.